Mechano-adaptive responses in the periodontium are coordinated by Wnt

Quanchen Xu*[1,2], Xue Yuan*[2], Xiaohui Zhang[2,3], Jinlong Chen[2,3], Yongxin Shi[2], John Brunski[2], and Jill A. Helms[2,§]

Appendix

Materials and Methods

Sample preparation, histology, enzymatic activity assays, immunohistochemistry, and histomorphometric analysis

Mandibles were harvested after sacrifice, bisected into hemi-mandibles, washed in phosphate buffer saline (PBS) and fixed in 4% paraformaldehyde (PFA) overnight. Following µCT imaging (below), samples were transferred to a microwave oven (Ted Pella, Redding, CA), in which a circulating 10% ethylenediamine tetraacetic acid (EDTA) solution was held for decalcification. After ~2 weeks, decalcified tissues were paraffin-embedded and cut in the sagittal orientation into 8 µm-thick sections. Following studies were mainly focused on mandible first molar (mnM1).

To observe PDL morphology, Pentachrome staining was performed (Leucht et al. 2007). To visualize collagen organization, slides were stained with 0.1% sirius red (35780, Pfaltz & Bauer, CT) dissolved in a saturated picric acid solution. Viewing was performed under polarized light.

Alkaline phosphatase (ALP) and tartrate-resistant acid phosphatase (TRAP) staining were performed to evaluate the bone remodeling. To detect ALP activity, BCIP (Roche, 113832201) and NBT (Roche, 11383213001) were used according to the manufacturer's recommendation. TRAP staining was performed using a kit (386A, Sigma) according to the manufacturer's instructions.

Immunohistochemistry was carried out to evaluate the molecular response of PDL and the surrounding alveolar bone to hyper-occlusion as described (Lim et al. 2014). Primary antibodies included proliferating cell nuclear antigen (PCNA) (ab18197, Abcam), Osterix (ab22552, Abcam), green fluorescent protein (GFP) (2956S, Cell Signaling Technology), Periostin (ab14041, Abcam), Cathepsin K (ab188604, Abcam) and Type I Collagen (ab34710, Abcam). 40,6-diamidino-2-phenylindole (DAPI) staining was used for counterstaining. Terminal deoxynucleotidyl transferase dUTP nick end labeling (TUNEL) (C10619, Thermo Fisher) staining was used to detect cell apoptosis.

Micro-computed tomography (µCT)

Parameter settings of scanning and analyses followed published guidelines (Bouxsein et al. 2010). Three-dimensional µCT imaging was performed with samples from tooth extraction and intact groups. Briefly, after being fixed in 4% PFA at 4°C overnight and washed in PBS, the samples were kept in 70% ethanol solution and scanned with VivaCT40 data-acquisition system (Scanco, Brüttisellen, Switzerland) at 10.5µm voxel size (70kV, 115µA and 300ms integration time). After the scanning, the ISQ format raw data was extracted and saved as image sequences in BMP format using ImageJ

(NIH, Bethesda, MD) software. Dataviewer (SkyScan) software were used to adjust the orientation of images. Dark (HA value: 0.75 g/cc) and light (HA value: 0.25g/cc) cylinder phantoms were scanned in advance, and the calibration of the reconstructed gray-scale attenuation values against mineral density was performed using CTAn software (SkyScan, Belgium). After calibration, regions of interest were set, then bone volume (BV) and total volume (TV) were evaluated. Segmentation of the alveolar bone and PDL was performed by automatically setting the gray-scale threshold and further verified slice by slice manually. Three-dimensional (3D) reconstruction and volume rendering were carried out using Avizo(FEI, Hillsboro, OR) and CTAn software.

Quantification of TUNEL and PCNA

Histomorphometry was performed using Image J software to quantify TUNEL^{+ve} and PCNA^{+ve} cells. To evaluate the number of TUNEL^{+ve} cells in the PDL, four mnM1 teeth and their surrounding tissues were selected from each group for analysis. The groups included 1) intact dentition; 2) hyper-loading group on day 1; 3) hyper-loading group on day 3; and 4) hyper-loading group on day 7, resulting in a total of 16 teeth used for analysis. For each tooth in each group, 3 sagittal tissue sections were analyzed and the number of TUNEL^{+ve} cells in the PDL occupying the furcation area was counted. The total number of DAPI^{+ve} viable cells in the same area was also counted; data were expressed as the number of TUNEL^{+ve} cells/total number of cells (%). Values were averaged between samples in each group, and standard deviation was calculated. The percentage of PCNA^{+ve} cells were determined using the same method.

Quantification of TRAP activity, ALP activity, and GFP staining

To determine the distribution of TRAP^{+ve} cells, four mnM1s were analyzed from each of the following four groups: 1) intact dentition; 2) hyper-loading group on day 3; 3) hyper-loading group on day 7; and 4) hyper-loading group on day 14; and hyper-loading group on day 28. A minimum of 3 representative tissue sections from each tooth was subjected to TRAP staining. Sections were imaged, and the pink/red pixels corresponding to TRAP activity were selected within a region of interest (ROI) using the ImageJ software, following methods outlined in (Sawyer et al. 2003). Total pixels within the same ROI was determined. TRAP activity/time was then expressed as the percentage of TRAP^{+ve} pixels/total pixels in the ROI which encompassed the interradicular alveolar bone. Quantification for ALP activity and the distribution of Wnt-responsive GFP^{+ve} cells were performed in the same manner following the method described in (Sawyer et al. 2003).

Quantification of PDL width

The width of the PDL in the furcation area was measured using two methods, one relying on histomorphometry and the other using µCT imaging. For the histomorphometric measurement, Periostin immunostaining images obtained from the midsagittal sections of each group were used as described (Fukui et al. 2003). The groups included: 1) intact dentition; 2) hyper-loading group on day 7; and 3) hyper-loading group on day 28. Four teeth from each group were analyzed and for each tooth, three midsagittal sections were chosen. A horizontal line was drawn from the crest of the interradicular alveolar bone parallel to the cementoenamel junction (CEJ) as described (Matsuda et al. 2018). The PDL width in this circumscribed area was then measured as the distance from the cementum at the furcation fornix to the horizontal line (indicated in Supplemental Fig. 1). Values were averaged, and standard deviation was calculated.

Measurements of the PDL width using μCT midsagittal images were performed for the same three groups using CTAn software (SkyScan) in the same manner.

Quantification of cusp height

To evaluate cusp abrasion on mnM1, four mnM1s were selected from each of the experimental groups e.g., intact dentition (5 weeks old), intact dentition (13 weeks old) and post extraction day 56 (13 weeks old) for a total of 12 samples. For each tooth, the cusp height was measured as described (Peretz et al. 1998). Briefly, the measurement was performed based on three-dimensional μCT imaging using Avizo software. Images of buccal side view were adopted, and the distances from the tip of the buccal-middle cusp to the cementoenamel junction were recorded. Measurements were averaged, and standard deviation was calculated. A one-way ANOVA was performed.

Hard tissue sections and quantification of mineral apposition rate (MAR)

Samples were fixed in 4% PFA overnight and dehydrated with 30% sucrose for 24 hours, then were processed for hard tissue embedding and sectioning using Kawamoto's method (Dyment et al. 2016; Kawamoto 2003). Briefly, the samples were embedded with SCEM embedding medium (Section Lab, Japan) and then sectioned with Cryofilm (Section Lab). The samples were then mounted with SCMM-R2 mounting medium (Section Lab). MAR was calculated by measuring the distance between the fluorochrome double-labeling lines in the alveolar bone, focusing on interradicular regions. A one-way ANOVA was performed to determine significance.

Human subject

The clinical image collection is approved by the Institutional review board (IRB) at Qingdao University.

Appendix Figures

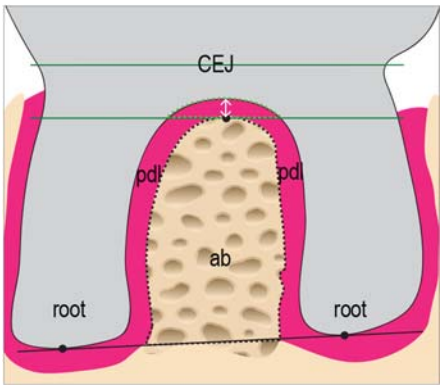

Supplemental Figure 1. Schematic representation of dental anatomy of furcation area and interradicular space. The green dotted area between the furcation fornix and the horizontal line across the crest of the alveolar bone parallel to the line across CEJ indicates the PDL of furcation area (PMID: 28944599). The white arrow indicates the PDL width of furcation area. The black dotted region indicates the alveolar bone in interradicular space. Abbreviations: ab, alveolar bone; pdl, periodontal ligament; CEJ, cemento-enamel junction.

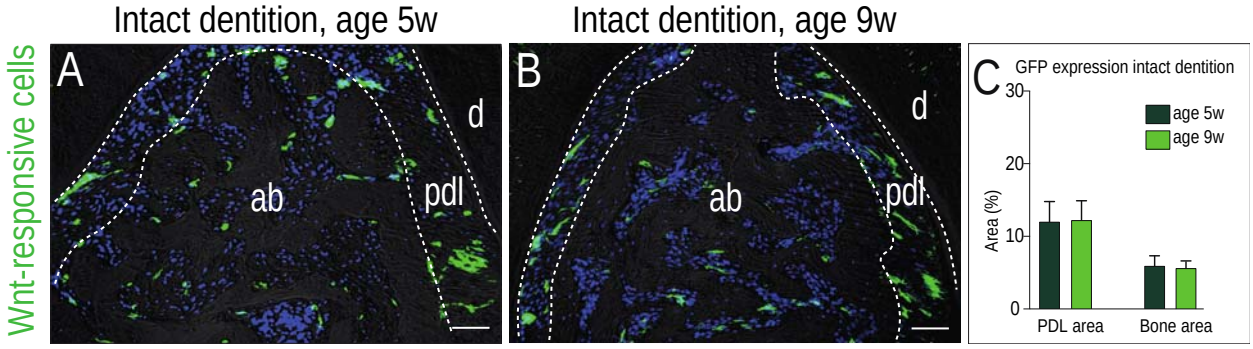

Supplemental Figure 2. Lineage tracing of Wnt-responsive cells in intact dentition group from (A) age 5w to (B) age 9w. (C) The quantification of GFP expression shows there is on significant difference of Wnt-responsive cells during this 28-day tracing. Abbreviations: ab, alveolar bone; pdl, periodontal ligament; d, dentin. Scale bars = 50 μm.

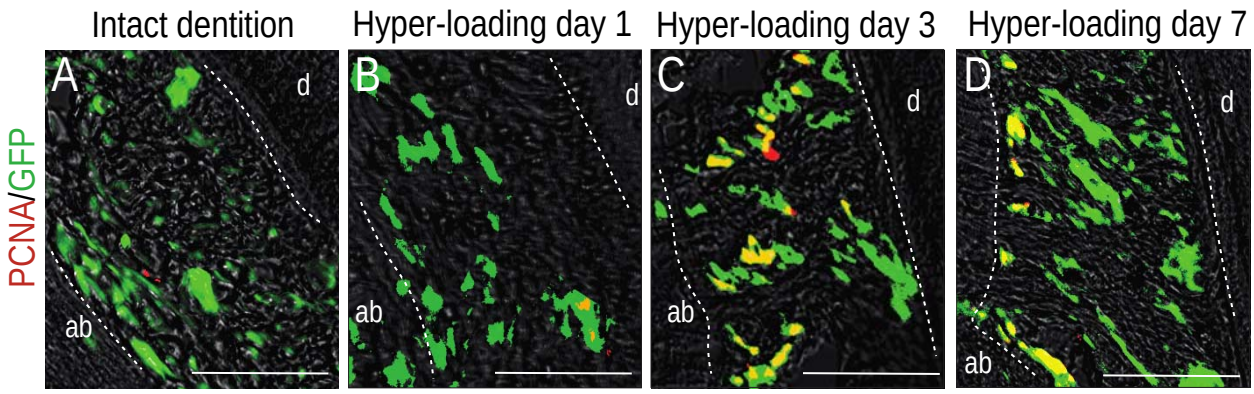

Supplemental Figure 3. Co-immunostaining with GFP and PCNA in (A) intact dentition, (B) hyper-loading group on day 1, (C) hyper-loading group on day3 and (D) hyper-loading group on day 7. Abbreviations: ab, alveolar bone; d, dentin. Scale bars = 50 μm.

Appendix Table

Table 1. Body weight (g) was checked weekly for both groups and no significant weight difference were found between experimental group and control group.

Group	Days after tooth extraction					
	Day 0	Day 7	Day 14	Day 21	Day28	Day 56
Intact	20.0±1.0	21.4±2.4	22.6±2.7	23.8±2.2	25.7±1.9	31.3±2.0
Hyper-loading	19.6±2.5	21.7±2.2	22.9±2.0	23.6±1.5	25.9±2.0	31.6±1.6

Appendix References

Bouxsein ML, Boyd SK, Christiansen BA, Guldberg RE, Jepsen KJ, Muller R. 2010. Guidelines for assessment of bone microstructure in rodents using micro-computed tomography. J Bone Miner Res. 25(7):1468-1486.

Dyment NA, Jiang X, Chen L, Hong SH, Adams DJ, Ackert-Bicknell C, Shin DG, Rowe DW. 2016. High-throughput, multi-image cryohistology of mineralized tissues. J Vis Exp. (115).

Fukui T, Yamane A, Komatsu K, Chiba M. 2003. Restoration of mechanical strength and morphological features of the periodontal ligament following orthodontic retention in the rat mandibular first molar. Eur J Orthod. 25(2):167-174.

Kawamoto T. 2003. Use of a new adhesive film for the preparation of multi-purpose fresh-frozen sections from hard tissues, whole-animals, insects and plants. Arch Histol Cytol. 66(2):123-143.

Leucht P, Kim JB, Wazen R, Currey JA, Nanci A, Brunski JB, Helms JA. 2007. Effect of mechanical stimuli on skeletal regeneration around implants. Bone. 40(4):919-930.

Lim WH, Liu B, Cheng D, Williams BO, Mah SJ, Helms JA. 2014. Wnt signaling regulates homeostasis of the periodontal ligament. J Periodontal Res. 49(6):751-759.

Matsuda Y, Minagawa T, Okui T, Yamazaki K. 2018. Resveratrol suppresses the alveolar bone resorption induced by artificial trauma from occlusion in mice. Oral Dis. 24(3):412-421.

Peretz B, Nevis N, Smith P. 1998. Morphometric analysis of developing crowns of maxillary primary second molars and permanent first molars in humans. Arch Oral Biol. 43(7):525-533.

Sawyer A, Lott P, Titrud J, McDonald J. 2003. Quantification of tartrate resistant acid phosphatase distribution in mouse tibiae using image analysis. Biotechnic & histochemistry : official publication of the Biological Stain Commission. 78(5):271-278.